Article

Not peer-reviewed version

Gold Nanoprobes for Detection of a Crucial EGFR Deletion for Early Diagnosis of Non-small Cell Lung Cancer

Maria Enea , Anupong Nuekaew , Ricardo Franco * , Eulália Pereira *

Posted Date: 6 March 2024

doi: 10.20944/preprints202403.0287.v1

Keywords: gold nanoprobe; DNA detection; EGRF mutation; non-cross linking; UV-Vis

 doi:10.20944/preprints202403.0287.v1

Article

Gold Nanoprobes for Detection of a Crucial EGFR Deletion for Early Diagnosis of Non-Small Cell Lung Cancer

Maria Enea [1,*], Anupong Nuekaew [1], Catarina Lemos [1], Ricardo Franco [2,3,*] and Eulália Pereira [1]

[1] LAQV /REQUIMTE, Departamento de Química e Bioquímica, Faculdade de Ciências, Universidade do Porto, Rua Campo Alegre, 687, Porto, 4169-007, Portugal; menea@fc.up.pt (M.E); anue279@aucklanduni.ac.nz (A.N); up201805232@edu.fc.up.pt (C.L); eulalia.pereira@fc.up.pt (E.P)

[2] Associate Laboratory i4HB—Institute for Health and Bioeconomy, Faculdade de Ciências e Tecnologia, Universidade NOVA de Lisboa, 2819-516 Caparica, Portugal; ricardo.franco@fct.unl.pt (R.F)

[3] UCIBIO –Applied Molecular Biosciences Unit, Departamento de Química, Faculdade de Ciências e Tecnologia, Universidade NOVA de Lisboa, 2819-516 Caparica, Portugal.; ricardo.franco@fct.unl.pt (R.F)

* Correspondence: ricardo.franco@fct.unl.pt

Abstract: Gold nanoparticles (AuNPs) exhibit improved optical and spectral properties compared to bulk materials, making them suitable for detection of DNA, RNA, antigens, and antibodies. Here, we describe a simple, selective, and rapid non-cross linking detection assay, using approx. 35 nm spherical Au nanoprobes, for a common mutation occurring in exon 19 of the epidermal growth factor receptor (EGFR), associated with non-small cell lung cancer cells. AuNPs were synthesized based on the seed-mediated growth method and functionalized with a specific 16 bp thiolated oligonucleotide using a pH-assisted method. Both AuNPs and Au nanoprobes proved to be highly stable and monodisperse by ultraviolet-visible spectrophotometry, dynamic light scattering (DLS) and electrophoretic light scattering (ELS). Our results indicate a detection limit of 1.5 μg mL^{-1} using a 0.15 nmol dm^{-3} Au nanoprobe concentration. In conclusion, this work is an effective possibility for a straight-forward, fast, and inexpensive alternative for the detection of DNA sequences related to lung cancer, leading to a potential platform for an early diagnosis of lung cancer patients.

Keywords: gold nanoprobe; DNA detection; EGRF mutation; non-cross linking; UV-Vis

1. Introduction

Gold nanoparticles (AuNPs), known for their biocompatibility and stability, find extensive applications in drug delivery and biosensing.[1–5] Their capacity to directly conjugate with various biomolecules, including proteins, drugs, antibodies, and nucleic acids, enhances the potential for diverse biomedical applications.[6,7] The high surface-to-volume ratio of AuNPs facilitates effective conjugation, and their localized surface plasmon resonance (LSPR) sensitivity to size and shape enhances the performance of colorimetric biosensors. Recently, the exponential increase in the use of AuNPs in sensor development has led to improved sensitivity, selectivity, and the simplification of analysis procedures, revolutionizing biodetection methods.[6,8–13]

Lung cancer is a prevalent form of primary malignant tumors leading to high mortality rates globally.[14,15] In recent decades, the number of deaths attributed to lung cancer worldwide has exceeded one million annually.[15] In many countries, the number of deaths from lung cancer exceeds those caused by other common types of cancer, mainly due to the absence of detectable symptoms. The clinical diagnosis of lung cancer heavily relies on expensive and invasive imaging techniques such as computed tomography (CT), magnetic resonance imaging (MRI), X-ray, and positron emission tomography (PET). [14] These methods are costly and present challenges in terms of speed, non-invasiveness, and early detection. Furthermore, they can have adverse effects in the

 doi:10.20944/preprints202403.0287.v1

human health and are inaccessible for low-cost screening with direct impact on the survival outcome.[14,16] Consequently, there is an urgent need to complement the existing methods with simpler, less expensive, and less invasive methods.

Non-small cell lung cancer (NSCLC) is the most common type of lung cancer. Researchers have found a promising approach to treat NSCLC by targeting epidermal growth factor receptor (EGFR) in patients. Tyrosine kinase inhibitors (TKIs), such as gefitinib or erlotinib, were used and show effectiveness in curing patients associated with this type of cancer.[17,18] Specifically, NSCLC patients with certain mutations in the EGFR protein have shown very good responses to TKIs. [19] The most common mutations in the EGFR gene occur in specific parts of the gene called exon 18–21. These mutations, frequently found in NSCLC patients, include deletions in exon 19 and a specific change known as the L858R mutation in exon 21. These mutations are strongly associated with a better response to TKIs in lung cancer patients.[20] Recent studies have shown that lung cancer patients with the exon 19 deletion mutation tend to have longer survival than those with the L858R mutation, when treated with drugs like gefitinib or erlotinib. [21] Knowing the mutation state of EGFR is thus essential in predicting how well a patient will respond to TKIs.

The current method of directly sequencing exon 18-21 of the EGFR gene from cancer samples is time-consuming and expensive due to the need for multiple steps and DNA amplification. So, it is critical to develop effective and fast methods to detect these mutations. A promising strategy is to use detection methods based on optical and aggregation properties of AuNPs that are highly affected by the size and shape of AuNPs. [9,22–25]. Among many morphologies and sizes, spherical 35 nm AuNPs are expected to present an increase detection sensitivity, as they present a high extinction coefficient, and therefore a more intense color than the most common 15 nm AuNPs. In addition, the lower curvature of these AuNPs is expected to increase the number and stability of interactions with the target.[9] The present work is focused on developing 35 nm Au nanoprobes for optical detection of an EGFR mutation associated to lung cancer. For this purpose, AuNPs were functionalized with a thiol-modified oligonucleotide and the Au nanoprobes were tested using a non-cross-linking approach for discrimination among different 84-100 bp-long synthetic DNA targets.

2. Materials and Methods

2.1. Au Nanoprobe Synthesis

2.1.1. Au Nanoparticles Synthesis and Characterization

Spherical-shaped AuNPs (35 nm) were synthesized based on a seed-mediated method described by Bastus et al.[26] First, a seed solution was prepared by addition, under heating and continuous stirring, of 1 mL of 25 mmol dm^{-3} $HAuCl_4$ to 150 mL of 2.2 mmol dm dm^{-3} sodium citrate solution, and the mixture was refluxed for 10 min. Then the mixture was cooled to 90 °C, and three growth steps were performed by adding 1 mL of 25 mmol dm^{-3} $HAuCl_4$, and reflux for 30 min with continuous stirring. The resulting AuNPs were characterized by UV–vis spectroscopy (Figure 2) and their concentrations and diameters were calculated accordingly to the method of Haiss et al. [23] The concentrations of the stock suspension of AuNPs were 0.22 nmol dm^{-3}. Hydrodynamic diameter and size distribution was evaluated by Dynamic Light Scattering.

2.1.2. Functionalization

All ssDNA used in the current study (unmodified target DNA and thiol-modified ssDNA oligonucleotide) were purchased from STAB Vida, Lda. (Portugal). The thiol modification of the oligonucleotide was located at the 5′ end (Table 1). The functionalization of the AuNPs was performed based on a pH assisted method [27,28] and 10 different ratios oligonucleotide:AuNPs : 250, 500, 800, 1000, 1250, 1500, 1750, 2000, 2250, and 2500. [27,28] Briefly, 500 µL of 35 nm AuNPs were concentrated by centrifugation at 800 g for 12 min and the resulting AuNPs were mixed with the oligonucleotide at the desired ratio. After 1 h incubation, 8 µL of 500 mmol dm^{-3} pH 3 citrate/ citric acid buffer was gradually added and incubated for 1 h. Finally, the mixture was washed by

 doi:10.20944/preprints202403.0287.v1

centrifugation at 800 g (10 min) and resuspended in 10 mmol dm^{-3} phosphate buffer (pH 8). All solutions were stored in the dark at 4 °C. UV–vis spectroscopy and characterization with DLS and gel agaroses was routinely performed in the optimization procedure.

Table 1. Sequences of the thiol-modified oligonucleotide used for AuNPs functionalization and of synthetic DNA targets.

Oligonycleotide	Length (bp)	Sequence 5′to 3′
Thiol-modified oligonucleotide	16	**SH-C6-CCTTAATTCTCTTCGT**
Normal DNA	100	GAG TGT AGC TCC TAA AGG AAC AAC CGA AAA GCC TCT ACA **ACGAAGAGAATTAAGG** AAC TAT CGC TGC CCT TAA AAT TGA AAG AGT GGA AGA CCT AGG TCT
Deleted DNA	84	GAG TGT AGC TCC TAA AGG AAC AAC CGA AAA GCC TCT ACA **()** AAC TAT CGC TGC CCT TAA AAT TGA AAG AGT GGA AGA CCT AGG TCT
Noncomplementary random DNA	84	CTTAGACCCTACAATGTACTAGTAGGCCTCTGCGCTGGCAATACAGATAA GATAATGTAGTCCCTGGCCTCAAAGGAACTCTCC

2.2. Au Nanoprobe Characterization

2.2.1. Gel Electrophoresis

An agarose gel of concentration 0.3% w/v was prepared by dissolving agarose in 1:8 TAE (pH 8.0). Following jellification, 10 µL samples were loaded into each lane, and the gel was run at 120 V for 20 min in the same running buffer. The images of the gel after the run were taken using an Apple iPhone 11 camera, to register the relative positions of the AuNP-derived bright red bands.

2.2.2. UV–Vis Analysis

Attenuance spectra for all samples were obtained using UV–vis spectrophotometer (Genesys 10S UV-Vis spectrophotometer). All spectra were run at room temperature at a wavelength ranging from 400 to 900, using quartz cells with a 1 cm path length (Hellma). Analysis of AuNPs stock, included a prior dilution with milli-Q water (dilution factor of 4). Unless otherwise stated, all nanoprobe sample was diluted in 10 mmol dm^{-3} phosphate buffer pH 8, prior to the measurement for a final concentration of 0.15 nmol dm^{-3}.

2.2.3. Dynamic Light Scattering and Electrophoretic Light Scattering:

The hydrodynamic diameter and zeta potential measurements were performed using a Malvern Zetasizer Nano ZS (Malvern, UK). An average of five measurements for each sample were taken at 25 °C, with light detection at 173° (DLS) and 17° (ELS). Solutions dilutions and buffer conditions were as in 2.2.2 UV-Vis analysis.

2.23. Non-Cross-Linking Detection Assay

The Au nanoprobes at a final concentration of 0.15 nmol dm^{-3} were incubated with the synthetic DNA target in 10 mmol dm^{-3} phosphate buffer (pH 8). Three types of DNA target were used: a total complementary sequence to the Au nanoprobe (normal DNA), a mutated deleted DNA that is noncomplementary to the nanoprobe, and a total random noncomplementary sequence to the nanoprobe. The target DNA concentrations used in the test ranged from 1.5 to 36 µg mL^{-1}. The assay

 doi:10.20944/preprints202403.0287.v1

mixtures were heated at 39 °C and left to cool down at room temperature for 10 min for optimal hybridization. Following, $MgCl_2$ was added and left for 10 min at room temperature to trigger aggregation of the Au nanoprobes in the presence of different DNA targets. All samples were analyzed visually and by UV–vis spectroscopy. A Blank was used containing the Au nanoprobe and the $MgCl_2$ salt in the corresponding concentration (no DNA target) and another control "Au nanoprobe" containing the Au nanoprobe alone (no salt, no DNA target).

From all spectra, a ratio of $Abs_{\lambda non\text{-}aggregated}/Abs_{\lambda aggregated}$ was calculated for as herein described: first, the spectrum of the non-aggregated sample (Au nanoprobe) was subtracted from the spectrum of the aggregated sample (blank control) and the minimum and maximum extinction values were determined. The minimum value corresponds to the wavelength of the non-aggregated state whereas the maximum value corresponds to the wavelength of the aggregated state. These wavelengths were then employed for measuring the colorimetric response for each sample as the ratio of the extinction peak of the non-aggregated nanoparticles (the minimum) to the characteristic extinction peak of the aggregated nanoparticles (the maximum), that is, $Abs_{\lambda non\text{-}aggregated}/Abs_{\lambda aggregated}$.

2.3. Statistical Analysis:

All statistical calculations were performed using the GraphPad Prism 9 software (GraphPad Software, San Diego, CA, USA). The results are presented as mean ± standard deviation (SD) from at least three independent experiments. To statistically compare the normal with the mutated/deleted DNA samples, the unpaired student t-test was used. Normality of the data distribution was assessed by the Kolmogorov–Smirnov, D'Agostino & Pearson, and Shapiro–Wilk tests. Significance was accepted at p values <0.05.

3. Results and Discussion

The discrimination assay between complementary (normal) and mutated/noncomplementary sDNA is based on the detection scheme depicted in Figure 1. The 16-mer oligonucleotide used to functionalize AuNPs is totally complementary to the normal DNA sequence and noncomplementary to the DNA sequence presenting an exon 19 deletion. Au nanoprobes were hybridized to DNA targets and controls, and after hybridization the resistance to salt-induced aggregation was assessed by UV/vis spectroscopy. The expected outcome is the following (see Figure 1): i) Upon hybridization with totally complementary DNA (normal), Au nanoprobes become resistant to salt-induced aggregation, so no significant changes are detected in the plasmon band. ii) For the deleted DNA, the negative control (non-complementary DNA) and for the blank (absence of DNA target), Au nanoprobes aggregate upon salt addition. The solution changes its color from red to blue, due to the appearance of a new LSPR band at higher wavelengths (ca. 700 nm). iii) The degree of aggregation can be assessed by the ratio between absorbance at the wavelength corresponding to LSPR of the aggregates and the absorbance at the wavelength of the LSPR of non-aggregated Au nanoprobes.

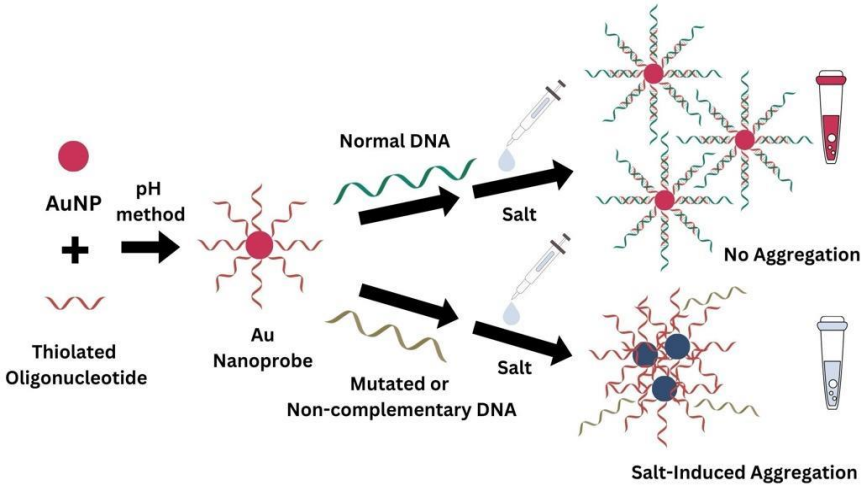

 doi:10.20944/preprints202403.0287.v1

Figure 1. The detection assay is based on the aggregation state of Au nanoprobes in the presence of target DNA that is complementary or noncomplementary (deleted) or in the absence of target DNA (blank), after addition of salt.

3.1. Au Nanoprobe Functionalization

3.1.1. Synthesis and Characterization of the 35nm AuNPs Stock

There are many well-established methods to synthesize spherical AuNPs, with reliable and repeatable results, enabling a good control of their shape and size. Most of them are based on the chemical reaction between chloroauric acid ($HAuCl_4$) and sodium citrate, imparting a negatively charged surface to the synthesized Au nanospheres.[26] In this work, we have chosen a seed-mediated growth method, that provides AuNPs with the desired diameter, with excellent size dispersion. [26]

The 35 nm AuNPs used have a Localized Surface Plasmon Resonance (LSPR) band centered around 525 nm (Figure S1), as expected for spherical AuNP of this diameter [23,26]. The lack of secondary bands indicates the absence of aggregates. The calculated size of the three batches of AuNPs from the UV-Vis spectra by using the formula of Haiss et al.[23] gives an average size around 35 nm. The hydrodynamic diameter by Intensity obtained through DLS analysis is overall slightly higher compared with the one obtained from UV-Vis with the use of method of Haiss et al. as it would be expected due to the influence of the citrate as capping agent. The associated polydispersity (*Đ*) is in the 0.17-0.21 range, indicating good monodispersity of the stock suspension. As expected, zeta potentials are negative and lower than -30 mV, indicating good colloidal stability.

Table 2. AuNPs characterization through UV-Vis, DLS and ELS analysis.

Batch	Diameter (nm)			Zeta Potential
	UV-Vis[1]	DLS[2]		
		Hydrodinamic diameter[2]	Polydispersity (Đ)	
1	37	38	0.19	-34.7 ± 1.3
2	36	41	0.21	-32.7 ± 1.0
3	35	36	0.17	-34.2 ± 1.5

[1] Calculated using the formula of Haiss el al. [23]. [2] Hydrodynamic diameter presented as Z Average by Intensity.

3.1.2. Successful Functionalization of AuNPs

Forty nm AuNPs were functionalized based on a pH method with different molar ratios of a thiol-modified 16-mer oligo nucleotide and the state of aggregation of the resulting probes was assessed by UV/vis spectroscopy (Figure 2A).

Spectra of the functionalized AuNPs are shown in Figure 2. It can be noticed that the oligonucleotide:AuNP ratio of 250 (Figure 2A) resulted in low extinction and/or presence of a secondary extinction band at higher wavelengths, indicating an inefficient functionalization process, and causing significant aggregation and/or loss of AuNPs. For ratios equal or higher than 500 (Figure 2A), the small shift in the maximum extinction wavelength from 525 nm (citrate-AuNPs) to 527 nm (Au nanoprobe) can be attributed to the adsorption of oligonucleotide.[9] Also, the shape and wavelength of the LSPR band also indicates that functionalization was successful, as no aggregation or significant loss of AuNPs occurred during the process. Therefore, functionalization with oligonucleotide:AuNP ratios of 500 or higher, seems promising without signs of aggregation of the obtained Au nanoprobes. These results are supported by agarose gel electrophoresis, where migration without signs of aggregation can be observed starting from ratio 500 (Figure 2B).

Preprints.org (www.preprints.org) | NOT PEER-REVIEWED | Posted: 6 March 2024 doi:10.20944/preprints202403.0287.v1

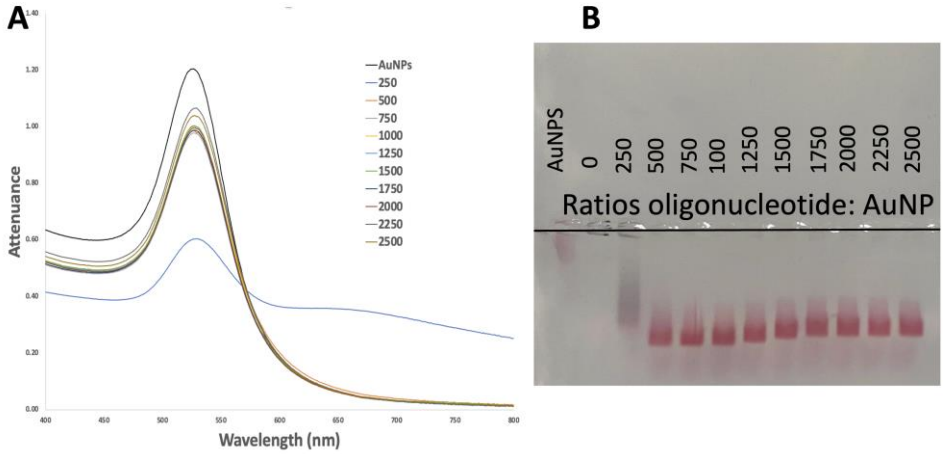

Figure 2. UV-Vis spectra (A) and agarose gel electrophoresis (B) of 35 nm AuNPs functionalized by the pH method using molar ratios of oligo/AuNPs in the 250-2500 range.

DLS measurements confirmed the results from UV-Vis. The occurrence of aggregation can be seen at a oligonucleotide:AuNP ratio of 250 with a high polydispersity index (0.47) and hydrodynamic diameter much higher than for the non-aggregated samples (63.41 nm). For oligonucleotide:AuNP ratios equal or higher than 500, the hydrodynamic diameter presents values around 44-46 nm, all higher than the AuNPs stock, suggesting successful functionalization. The polydispersity index decreases with increasing ratios reaching desired polydispersity values below 0.2 at ratio oligos:AuNPs 1000, indicating a good monodispersity of the resulting probes prepared starting with this ratio or higher.

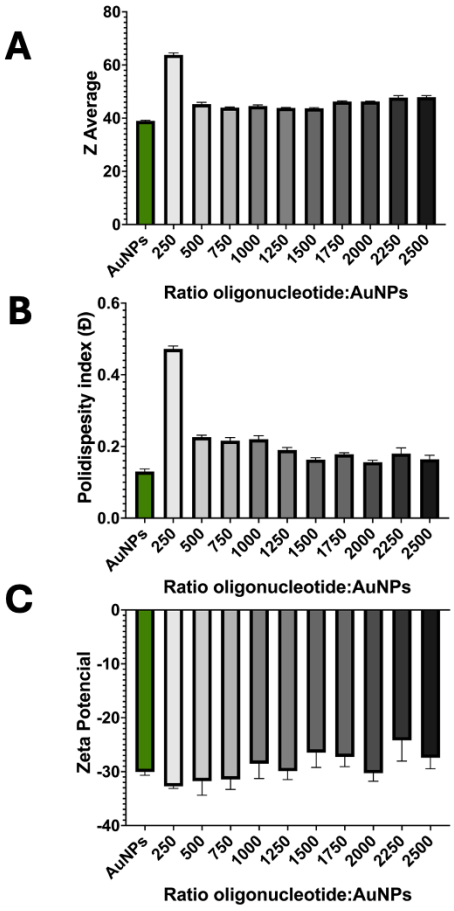

 doi:10.20944/preprints202403.0287.v1

Figure 3. Physical-chemical characterization of AuNPs and the gold nanoprobes with ratio oligonucleotides: AuNP between 250 and 2500: Zeta Average (A) and Polidispersity Index (B) from DLS analysis and Zeta Potential (C) from ELS analysis. Data presented as mean ± SD of at least three independent experiments.

Considering these results, we selected an oligonucleotide:AuNPs ratio of 1000 for further studies. Ratios between 500 and 750 demonstrated low reproducibility in the functionalization and inconsistent results in the detection assay (data not shown).

Thiol-modified oligonucleotides react with AuNPs through thiol/gold chemistry, but negative charges on both entities impair effective conjugation. Overcoming this requires challenging methods, particularly for larger AuNPs (>15 nm). [9,28–31]. The pH method used in our study proved to be optimal for functionalization of larger spherical AuNPs [9,27,28], as at low pH, two of the nucleobases (A and C) are protonated, making DNA less negatively charged, thus reducing DNA-AuNP and DNA−DNA repulsions. [28] Compared to other methods like salt-aging, pH-assisted functionalization offers two key benefits: higher efficiency and shorter processing time, taking hours instead of days.[27,28]

Oligonucleotide:AuNPs ratios selected in the current study, are in the range of published data for the functionalization of spherical AuNPs. The ratio used for Au nanoprobes is expected to be higher compared with smaller 15 nm AuNPs, and is associated to a decrease of curvature, affecting the interactions among the DNA strands, and consequently affecting the DNA density/loading on the surface of AuNPs compared to 15 nm AuNPs. [9,29] The ratio used in our current study is slightly smaller than the one used in our previous study, where a oligonucelotide:AuNP ratio of 1300 was used for functionalization of 35 nm spherical AuNPs using the pH-assisted functionalization.[9] However, since this method depends on protonation of specific DNA bases (A and C), variations in adenine and cytosine percentages between oligonucleotides may require different ratios. Additionally, their lengths are crucial for discrimination and stable Au nanoprobes, as shown previously. [9,27]

3.2. Detection Assay

UV-Vis spectra of 35 nm Au nanoprobes were obtained in the presence (Complementary/Mutated/Negative Control) or absence (Au nanoprobe, Blank) of DNA targets, after adding $MgCl_2$. When salt-induced aggregation occurs, as in the case of noncomplementary DNA or lack of any DNA target, a second plasmon band at higher wavelengths emerges. This occurs when noncomplementary DNA targets do not hybridize with any part of the Au nanoprobe's oligonucleotide, or when no DNA target is present, preventing protection against salt-induced aggregation. The second plasmon band at higher wavelengths is associated with a color change of the initial solution from red to blue-purple.

Complete hybridization of the DNA target with the Au nanoprobe's oligonucleotide results in high resistance against aggregation, maintaining the probe's initial red color and optical properties. A small shift in the plasmon band can occur, due to the presence of hybridized DNA near the Au nanoprobes surface.

UV/vis spectra also give information of the extent of aggregation, either directly by the extinction of the LSPR band of the aggregates or by calculating extinction ratios.[9] Ratios can be computed using LSPR maximum absorptions of non-aggregated vs. aggregated nanoparticles (AbsNon-Agg/AbsAgg). However, this overlooks variations in aggregation patterns influenced by AuNP size, DNA target length, and inducing salt type. Another method involves subtracting the non-aggregated sample spectrum from the aggregated one for each type of AuNPs. This yields minimum and maximum absorption wavelengths, marking the locations of non-aggregated and aggregated peaks. These values are then used to calculate AbsNon-Agg/AbsAgg ratios. The use of UV-Vis spectroscopy and calculation of aggregation ratios was previously proven to be an efficient tool in discrimination among DNA for non-crosslinking methods.[9–11], with different ratios corresponding to differences in the aggregation profile. The hybridization temperature was set based on the melting temperature

 doi:10.20944/preprints202403.0287.v1

of the oligonucleotide probe to ensure optimal conditions for hybridization with a perfectly complementary sequence to the exon 19 deletion mutation type. [9,32,33]

Figure 4 summarizes all results, with DNA targets at concentrations up to 36 μg mL^{-1} and seven $MgCl_2$ concentration (from 15 to 50 mM). Each bar represents differences in AbsNon-Agg/AbsAgg ratios between assays with complementary normal DNA and noncomplementary deleted targets, a measure of the discrimination of the assay. In Figure 4, we can notice a concentration dependent discrimination between normal and mutated DNA with an increase in the corresponding ratio difference with increase in the DNA target concentration, independent of the salt concentration used. This can be easily observed by the increasing size of bars as we go from the front to the back of the graph. This would be expected as the total complementary hybridize with the Au nanoprobe protecting against aggregation induced by $MgCl_2$ while the mutated form does not hybridize. The effect is also dependent on salt concentration, as differences in aggregation ratios increase with increasing salt concentrations, up to 20 mM. For higher salt concentrations there is a perceptible decrease of the difference in the ratios. This effect of increasing salt concentration can be observed by the varying size of bars of the same color (same DNA target concentration), from the left to the right of the graph. A $MgCl_2$ concentration of 20 mM is thus the optimal condition to discriminate between complementary and noncomplementary DNA targets.

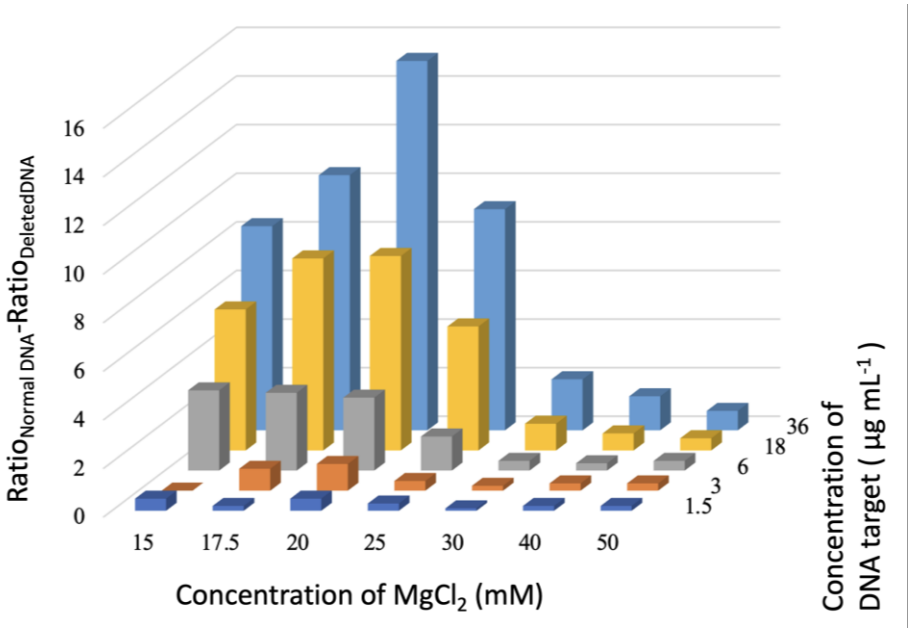

Figure 4. Ratio difference between ratio AbsNon-Agg/AbsAgg of normal DNA and deleted DNA at 1.5 (dark blue line), 3 (orange line), 6 (grey line), 18 (yellow line) and 36 (blue line) μg mL^{-1} and $MgCl_2$: 15, 17.5, 20, 25, 30, 40 and 50 mM.

Figure 5 presents a complete analysis of assays performed with Au nanoprobe incubated with target DNA at concentrations ranging from 1.5 to 36 μg mL^{-1} and for the optimal $MgCl_2$ concentration of 20 mM. Statistical analysis (Figure 5A) demonstrates that for all tested target DNA concentration, discrimination (i.e., AbsNon-Agg/AbsAgg ratio difference) is statistically significant. Furthermore, discrimination is directly proportional to DNA target concentration (inset in Figure 5A), and is revealed by visual inspection of the color of the solution for DNA target concentrations higher than 6 μg mL^{-1} (Figure 5B).

The observed statistically significance for discrimination, at all tested target DNA concentration, was observed for two other $MgCl_2$ concentrations, one below (15 mM) and the other above (50 mM) the optimal 20 mM value (Figure S5). These results corroborate a higher protection against aggregation for Au nanoprobes incubated with complete/normal DNA compared with mutated/deleted DNA. For all conditions, the calculated ratios for the deleted DNA is very close to the values obtained for non-complementary DNA and the lack of DNA (Figure S4) indicating they

 doi:10.20944/preprints202403.0287.v1

have similar aggregation profile in the tested conditions. The low protection against aggregation as in the case of deleted and noncomplementary DNA noticed after addition of $MgCl_2$, is associated to the lack of hybridization between the ssDNA on the surface of AuNPs and the DNA target presented in the solution. However, the behavior of normal/complete DNA differs across experimental conditions: the Au nanoprobe incubated with complete DNA consistently shows a higher ratio compared to mutated DNA in all tested conditions. Nonetheless, the ratio values vary significantly, suggesting different levels of protection against $MgCl_2$-induced aggregation or inadequate aggregation. For example, when 15 mM $MgCl_2$ is used, the difference between the ratio obtained for normal ssDNA and mutated ssDNA is low for all target DNA concentrations. Both normal ssDNA and mutated ssDNA show high ratios, leading to poor discrimination between normal and mutated DNA sequences. The discrimination between the two types of DNA target becomes significant only at 6 ng/µL (Figure S5). This can be additionally confirmed by naked eye observation: even at the highest target DNA concentration tested (36 µg mL^{-1}), samples remain red (data not shown). For $MgCl_2$ concentrations higher than 20 mM, the ratio difference started to decrease. This decrease is due to aggregation both in normal and deleted DNA samples, leading to a AbsNon-Agg/AbsAgg ratio ratio values lower than 3. Likewise, it can be observed visually that the signal differentiation is also more difficult, becoming impossible for 50 mM $MgCl_2$, where both samples are extensively aggregated already at the lowest target DNA concentration tested (6 µg mL^{-1}) (Figure S5).

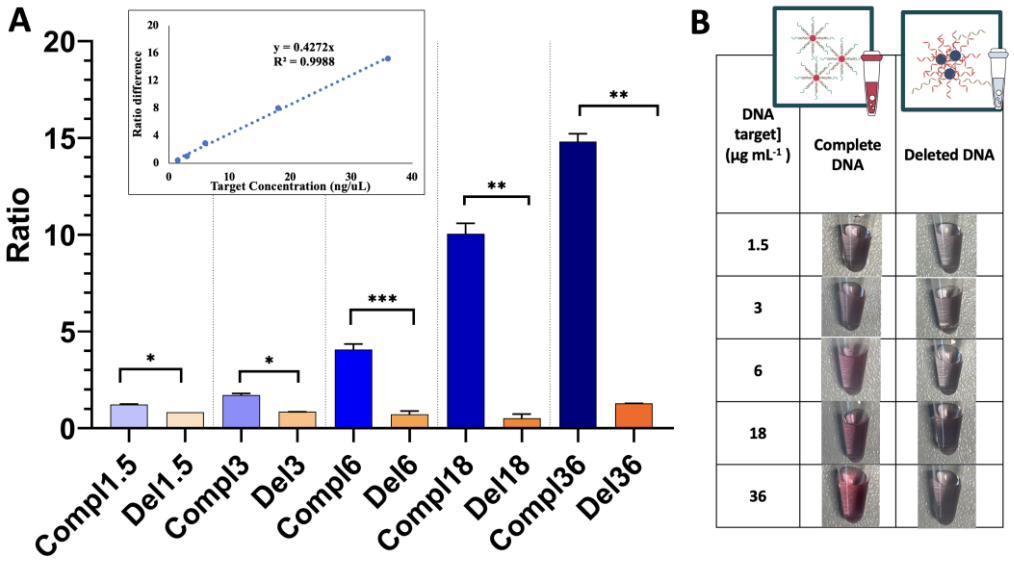

Figure 5. Analysis of Au nanoprobe incubated with target DNA at concentrations ranging from 1.5 to 36 µg mL^{-1} and 20mM $MgCl_2$. Representation of the Ratio AbsNon-Agg/AbsAgg of normal/complementary DNA (blue bars) and deleted DNA (orange bar), one asterisk indicating $p \leq 0.05$, two $p \leq 0.01$, three $p \leq 0.001$ and four asteriks indicating $p \leq 0.0001$ in cases of statistical significance (A), and dependence of the ratio difference between normal and deleted DNA (inset); and photographs of the Au nanoprobe mutated and target DNA of different concentrations (1.5 to 36 µg mL^{-1}) and 20 mM $MgCl_2$ (B).

4. Conclusions

In this work, we describe the use of 35 nm spherical Au–nanoprobe for direct discrimination of a deletion mutation associated to non-small cell lung cancer. Using a non-cross-linking method, we demonstrated that this Au–nanoprobe is capable of successfully discriminating among complementary (normal) DNA and deleted or random noncomplementary DNA target with a low discrimination limit of 1.5 µg mL^{-1}. This methodology has proven to be a reliable and robust screening technique that can accurately be used for DNA discrimination in controlled conditions. Results are obtained in a very short period (20 min) and the use of a spherical 35 nm Au–nanoprobe simplifies integration in a disposable device for use at the point of care test. Further optimization toward

 doi:10.20944/preprints202403.0287.v1

increased specificity in biological samples is still required before the technology can be translated to routine screening.

Supplementary Materials: The following supporting information can be downloaded at the website of this paper posted on Preprints.org. UV-Vis spectra of AuNPs and Au nanoprobes, alone and the latter also incubated with $MgCl_2$; DNA concentration dependent effect of the AbsNon-Agg/AbsAgg ratio for Au nanoprobes with three different targets and 7 different $MgCl_2$ concentrations, between 15 mM and 50 mM; and bar graph depicting differences in AbsNon-Agg/AbsAgg ratios between complementary DNA and deleted DNA targets tested for $MgCl_2$ concentrations 15 and 50 mM.

Author Contributions: Conceptualization, M.E, R.F. and E.P.; methodology, M.E, R.F and E.P.; software, M.E and A.N.; investigation, M.E, A.N and C.L.; resources, E.P.; data curation, M.E and A.N.; writing—original draft preparation, M.E.; writing—review and editing, R.F and E.P.; supervision, R.F and E.P.; funding acquisition, R.F and E.P. All authors have read and agreed to the published version of the manuscript.

Funding: This research was funded by Portuguese funds from Fundação para a Ciência e a Tecnologia, I.P. (FCT-MCTES) in the scope of projects UIDP/04378/2020; UIDB/04378/2020 of UCIBIO, UIDB/50006/2020 and UIDP/50006/2020 of LAQV and LA/P/0140/2020 of i4HB. M.E. acknowledged LAQV for her Post-Doc grant ref. REQUIMTE 2022-06 and A.N acknowledge the Erasmus+: Erasmus Mundus program of the European Union.

Acknowledgements: Dr. Orfeu Flores, and Carla Clemente, both from STABVida, Investigação e Serviços em Ciências Biológicas Lda., Portugal, are acknowledged for fruitful discussions leading to the definition of the assay target.

Conflicts of Interest: The authors declare no conflict of interest.

References

1. de Almeida, M.P.; Pereira, E.; Baptista, P.; Gomes, I.; Figueiredo, S.; Soares, L.; Franco, R. Gold nanoparticles as (bio) chemical sensors. In *Comprehensive analytical chemistry*; Elsevier: 2014; Volume 66, pp. 529-567.
2. Franco, R.; Pedrosa, P.; Carlos, F.F.; Veigas, B.; Baptista, P.V. Gold nanoparticles for DNA/RNA-based diagnostics. *Handbook of nanoparticles* **2015**, 1339.
3. Enea, M.; Araújo, A.M.; Almeida, M.P.; Soares, M.E.; Gonçalves-Monteiro, S.; Pinho, P.G.; Pereira, E.; Bastos, M.L.; Carmo, H. A Metabolomic Approach for the In Vivo Study of Gold Nanospheres and Nanostars after a Single-Dose Intravenous Administration to Wistar Rats. *Nanomaterials (Basel)* **2019**, *9*, doi:10.3390/nano9111606.
4. Enea, M.; Pereira, E.; Costa, J.; Soares, M.E.; Dias da Silva, D.; Bastos, M.L.; Carmo, H.F. Cellular uptake and toxicity of gold nanoparticles on two distinct hepatic cell models. *Toxicol In Vitro* **2021**, *70*, 105046, doi:10.1016/j.tiv.2020.105046.
5. Enea, M.; Pereira, E.; Silva, D.D.; Costa, J.; Soares, M.E.; de Lourdes Bastos, M.; Carmo, H. Study of the intestinal uptake and permeability of gold nanoparticles using both in vitro and in vivo approaches. *Nanotechnology* **2020**, *31*, 195102, doi:10.1088/1361-6528/ab6dfb.
6. Baptista, P.; Pereira, E.; Eaton, P.; Doria, G.; Miranda, A.; Gomes, I.; Quaresma, P.; Franco, R. Gold nanoparticles for the development of clinical diagnosis methods. *Analytical and bioanalytical chemistry* **2008**, *391*, 943-950.
7. Tomás, A.L.; de Almeida, M.P.; Cardoso, F.; Pinto, M.; Pereira, E.; Franco, R.; Matos, O. Development of a Gold Nanoparticle-Based Lateral-Flow Immunoassay for Pneumocystis Pneumonia Serological Diagnosis at Point-of-Care. *Front Microbiol* **2019**, *10*, 2917, doi:10.3389/fmicb.2019.02917.
8. Oliveira, M.J.; Caetano, S.; Dalot, A.; Sabino, F.; Calmeiro, T.R.; Fortunato, E.; Martins, R.; Pereira, E.; Prudêncio, M.; Byrne, H.J.; et al. A simple polystyrene microfluidic device for sensitive and accurate SERS-based detection of infection by malaria parasites. *Analyst* **2023**, *148*, 4053-4063, doi:10.1039/d3an00971h.
9. Enea, M.; Peixoto de Almeida, M.; Dias, A.; Ferreira, B.; Bernardes, C.; Flores, O.; Pereira, E.; Franco, R. Improved Gold Nanoprobes for Detection of Single Nucleotide Polymorphisms: The Influence of Size. *Particle & Particle Systems Characterization* **2022**, *39*, 2200137.
10. Baptista, P.; Doria, G.; Henriques, D.; Pereira, E.; Franco, R. Colorimetric detection of eukaryotic gene expression with DNA-derivatized gold nanoparticles. *Journal of biotechnology* **2005**, *119*, 111-117.
11. Carlos, F.F.; Flores, O.; Doria, G.; Baptista, P.V. Characterization of genomic single nucleotide polymorphism via colorimetric detection using a single gold nanoprobe. *Anal Biochem* **2014**, *465*, 1-5, doi:10.1016/j.ab.2014.07.019.
12. Doria, G.; Larguinho, M.; Dias, J.T.; Pereira, E.; Franco, R.; Baptista, P.V. Gold-silver-alloy nanoprobes for one-pot multiplex DNA detection. *Nanotechnology* **2010**, *21*, 255101, doi:10.1088/0957-4484/21/25/255101.

13. Eaton, P.; Doria, G.; Pereira, E.; Baptista, P.V.; Franco, R. Imaging gold nanoparticles for DNA sequence recognition in biomedical applications. *IEEE Trans Nanobioscience* **2007**, *6*, 282-288, doi:10.1109/tnb.2007.908985.
14. Lee, E.; Kazerooni, E.A. Lung Cancer Screening. *Semin Respir Crit Care Med* **2022**, *43*, 839-850, doi:10.1055/s-0042-1757885.
15. Thai, A.A.; Solomon, B.J.; Sequist, L.V.; Gainor, J.F.; Heist, R.S. Lung cancer. *Lancet* **2021**, *398*, 535-554, doi:10.1016/s0140-6736(21)00312-3.
16. Wu, F.Z.; Kuo, P.L.; Huang, Y.L.; Tang, E.K.; Chen, C.S.; Wu, M.T.; Lin, Y.P. Differences in lung cancer characteristics and mortality rate between screened and non-screened cohorts. *Sci Rep* **2019**, *9*, 19386, doi:10.1038/s41598-019-56025-6.
17. Takano, T.; Ohe, Y.; Tsuta, K.; Fukui, T.; Sakamoto, H.; Yoshida, T.; Tateishi, U.; Nokihara, H.; Yamamoto, N.; Sekine, I.; et al. Epidermal growth factor receptor mutation detection using high-resolution melting analysis predicts outcomes in patients with advanced non small cell lung cancer treated with gefitinib. *Clin Cancer Res* **2007**, *13*, 5385-5390, doi:10.1158/1078-0432.Ccr-07-0627.
18. Lynch, T.J.; Bell, D.W.; Sordella, R.; Gurubhagavatula, S.; Okimoto, R.A.; Brannigan, B.W.; Harris, P.L.; Haserlat, S.M.; Supko, J.G.; Haluska, F.G.; et al. Activating mutations in the epidermal growth factor receptor underlying responsiveness of non-small-cell lung cancer to gefitinib. *N Engl J Med* **2004**, *350*, 2129-2139, doi:10.1056/NEJMoa040938.
19. Paez, J.G.; Jänne, P.A.; Lee, J.C.; Tracy, S.; Greulich, H.; Gabriel, S.; Herman, P.; Kaye, F.J.; Lindeman, N.; Boggon, T.J.; et al. EGFR mutations in lung cancer: correlation with clinical response to gefitinib therapy. *Science* **2004**, *304*, 1497-1500, doi:10.1126/science.1099314.
20. Riely, G.J.; Pao, W.; Pham, D.; Li, A.R.; Rizvi, N.; Venkatraman, E.S.; Zakowski, M.F.; Kris, M.G.; Ladanyi, M.; Miller, V.A. Clinical course of patients with non-small cell lung cancer and epidermal growth factor receptor exon 19 and exon 21 mutations treated with gefitinib or erlotinib. *Clin Cancer Res* **2006**, *12*, 839-844, doi:10.1158/1078-0432.Ccr-05-1846.
21. Shigematsu, H.; Gazdar, A.F. Somatic mutations of epidermal growth factor receptor signaling pathway in lung cancers. *Int J Cancer* **2006**, *118*, 257-262, doi:10.1002/ijc.21496.
22. Hua, Y.; Chandra, K.; Dam, D.H.; Wiederrecht, G.P.; Odom, T.W. Shape-Dependent Nonlinear Optical Properties of Anisotropic Gold Nanoparticles. *J Phys Chem Lett* **2015**, *6*, 4904-4908, doi:10.1021/acs.jpclett.5b02263.
23. Haiss, W.; Thanh, N.T.; Aveyard, J.; Fernig, D.G. Determination of size and concentration of gold nanoparticles from UV-vis spectra. *Anal Chem* **2007**, *79*, 4215-4221, doi:10.1021/ac0702084.
24. Sousa, S.; Castro, A.; Correia da Costa, J.M.; Pereira, E. Biosensor based immunoassay: A new approach for serotyping of Toxoplasma gondii. *Nanomaterials* **2021**, *11*, 2065.
25. Esfahani, M.R.; Pallem, V.L.; Stretz, H.A.; Wells, M.J. Extinction, emission, and scattering spectroscopy of 5-50 nm citrate-coated gold nanoparticles: An argument for curvature effects on aggregation. *Spectrochim Acta A Mol Biomol Spectrosc* **2017**, *175*, 100-109, doi:10.1016/j.saa.2016.11.052.
26. Bastús, N.G.; Comenge, J.; Puntes, V. Kinetically controlled seeded growth synthesis of citrate-stabilized gold nanoparticles of up to 200 nm: size focusing versus Ostwald ripening. *Langmuir* **2011**, *27*, 11098-11105, doi:10.1021/la201938u.
27. Zhang, X.; Gouriye, T.; Goeken, K.; Servos, M.R.; Gill, R.; Liu, J. Toward fast and quantitative modification of large gold nanoparticles by thiolated DNA: scaling of nanoscale forces, kinetics, and the need for thiol reduction. *The Journal of Physical Chemistry C* **2013**, *117*, 15677-15684.
28. Zhang, X.; Servos, M.R.; Liu, J. Instantaneous and quantitative functionalization of gold nanoparticles with thiolated DNA using a pH-assisted and surfactant-free route. *Journal of the American Chemical Society* **2012**, *134*, 7266-7269.
29. Hurst, S.J.; Lytton-Jean, A.K.; Mirkin, C.A. Maximizing DNA loading on a range of gold nanoparticle sizes. *Anal Chem* **2006**, *78*, 8313-8318, doi:10.1021/ac0613582.
30. Mirkin, C.A.; Letsinger, R.L.; Mucic, R.C.; Storhoff, J.J. A DNA-based method for rationally assembling nanoparticles into macroscopic materials. *Nature* **1996**, *382*, 607-609, doi:10.1038/382607a0.
31. Liu, B.; Liu, J. Freezing-Driven DNA Adsorption on Gold Nanoparticles: Tolerating Extremely Low Salt Concentration but Requiring High DNA Concentration. *Langmuir* **2019**, *35*, 6476-6482, doi:10.1021/acs.langmuir.9b00746.
32. Soares, L.; Csáki, A.; Jatschka, J.; Fritzsche, W.; Flores, O.; Franco, R.; Pereira, E. Localized surface plasmon resonance (LSPR) biosensing using gold nanotriangles: detection of DNA hybridization events at room temperature. *Analyst* **2014**, *139*, 4964-4973.
33. Lee, H.; Kang, T.; Yoon, K.-A.; Lee, S.Y.; Joo, S.-W.; Lee, K. Colorimetric detection of mutations in epidermal growth factor receptor using gold nanoparticle aggregation. *Biosensors and Bioelectronics* **2010**, *25*, 1669-1674.

 doi:10.20944/preprints202403.0287.v1